Effect of temperature on the formation of highly oxygenated organic molecules (HOM) from alpha-pinene ozonolysis

Lauriane L. J. QUÉLÉVER [1], Kasper KRISTENSEN [2*], Louise NORMANN JENSEN [2], Bernadette ROSATI [2,3], Ricky TEIWES [2,3], Kaspar R. DAELLENBACH [1], Otso PERÄKYLÄ [1], Pontus ROLDIN [4], Rossana BOSSI [5], Henrik B. PEDERSEN [3], Marianne GLASIUS [2], Merete BILDE [2] and Mikael EHN [1].

[1] Institute for Atmospheric and Earth System Research – INAR / Physics, P.O. Box 64, FI-00014 University of Helsinki, Finland.

[2] Aarhus University, Department of Chemistry, Langelandsgade 140, DK-8000 Aarhus C, Denmark.

[3] Aarhus University, Department of Physics and Astronomy, Ny Munkegade 120, DK-8000 Aarhus C, Denmark.

[4] Lund University, Division of Nuclear Physics, P.O. Box 118, SE-22100 Lund, Sweden.

[5] Aarhus University, Department of Environmental Science – Atmospheric Chemistry and Physics, Frederiksborgvej 399, DK-4000 Roskilde, Denmark.

[*] Presently at University of California, Department of Environmental Science, Policy and Management, Hilgard Hall 251B, CA-94720-3114 Berkeley, United States of America.

Correspondence to Lauriane L. J. QUÉLÉVER (Lauriane.quelever@helsinki.fi) & Mikael EHN (Mikael.ehn@helsinki.fi)

Abstract

Highly-oxygenated organic molecules (HOM) are important contributors to Secondary Organic Aerosol (SOA) and New-Particle Formation (NPF) in the boreal atmosphere. This newly discovered class of molecules is efficiently formed from atmospheric oxidation of biogenic volatile organic compounds (VOC), such as monoterpenes, through a process called autoxidation. This process, in which peroxy-radical intermediates isomerize to allow addition of molecular oxygen, is expected to be highly temperature-dependent. Here, we studied the dynamics of HOM formation during α-pinene ozonolysis experiments performed at three different temperatures, 20 °C, 0 °C and -15 °C, in the Aarhus University Research on Aerosol (AURA) chamber. We found that the HOM formation, under our experimental conditions (50 ppb α-pinene, 100 ppb ozone), decreased considerably as temperature decreased, with molar yields dropping by around a factor of 50 when experiments were performed at 0 °C, compared to 20 °C. At -15 °C, the HOM signals were already close to the detection limit of the nitrate-based Chemical Ionization Atmospheric Pressure interface Time Of Flight (CI-APi-TOF) mass spectrometer used for measuring gas-phase HOM. Surprisingly, very little difference was seen in the mass spectral distribution of the HOM molecules of interest at 0 °C and 20 °C, with e.g. the ratios between the typical HOM products $C_{10}H_{14}O_7$, $C_{10}H_{14}O_9$, and $C_{10}H_{14}O_{11}$ remaining fairly constant. The more oxidized species have undergone more isomerization steps, yet, at lower temperature, they did not decrease more than the less oxidized species. One possible explanation is be that the rate-limiting step forming these HOM occurs before the products become oxygenated enough to be detected by our CI-APi-TOF (i.e. typically seven or more oxygen atoms). The strong temperature dependence of HOM formation was observed under temperatures highly relevant for the boreal forest, but the exact magnitude of this effect in the atmosphere will be much more complex: the fate of peroxy-radicals is a competition between autoxidation (influenced by temperature and VOC type) and bimolecular termination pathways (influenced mainly by concentration of reaction partners). While the temperature influence is likely smaller in the boreal atmosphere than in our chamber, the magnitude and complexity of this effect clearly deserves more consideration in future studies in order to estimate the ultimate role of HOM on SOA and NPF under different atmospheric conditions.

Keywords: HOM formation & yield, Temperature, ACCHA campaign, AURA chamber, Mass Spectrometry, CI-APi-TOF

1. Introduction

Aerosol particles impact Earth's climate by scattering and absorbing solar radiation, and by influencing cloud properties when they act as Cloud Condensation Nuclei (CCN) (IPCC, 2013). Organic compounds contribute significantly to the chemical composition of aerosol, accounting from 20 % to 90 % of the total aerosol mass of sub-micrometer particles depending on their location in the globe (Jimenez et al., 2009). Submicron organic aerosol are dominantly secondary. Called Secondary Organic Aerosol (SOA), they originate from gas-to-particle conversion from condensable vapors (Hallquist et al., 2009; Zhang et al., 2007). These vapors are mainly oxidation products of Volatile Organic Compounds (VOC), having sufficiently low vapor pressure (i.e. volatility) to condense onto aerosol particles (Hallquist et al., 2009).

In order to interact efficiently with solar radiation or to activate cloud droplets, aerosol particles need to be around 100 nm in diameter or larger (Dusek et al., 2006). If particles have formed through nucleation processes in the atmosphere (e.g. Kulmala et al., 2013), their ability to grow to climate-relevant sizes before being scavenged through coagulation is critically impacted by the rate at which low-volatile vapors will condense onto them (Donahue et al., 2013). Extremely Low-Volatile Organic Compounds (ELVOC), introduced by Donahue et al. (2012), have the ability to condense irreversibly onto even the smallest aerosol particles and clusters and thus contribute to particle growth. Low-Volatile Organic Compounds (LVOC), typically more abundant in the atmosphere, are important for the growth of particles larger than a few nanometers (Tröstl et al., 2016).

Highly-oxygenated Organic Molecules (HOM, Ehn et al., 2014 & 2017; Bianchi et al., 2019) were recently identified as a large contributor to (E)LVOC and the growth of newly formed particles (Ehn et al., 2014; Tröstl et al., 2016). First observed in measurements of naturally charged ions in the boreal forest (Ehn et al., 2010 &

2012) using the Atmospheric Pressure interface Time Of Flight (APi-TOF) mass spectrometer (Junninen et al., 2010), HOM quantification only became possible through the application of nitrate ion chemical ionization (CI) mass spectrometry (Zhao et al., 2013; Ehn et al., 2014). Most studies have utilized the APi-TOF coupled to such a chemical ionization source (CI-APi-TOF, Jokinen et al., 2012), and detailed laboratory studies have been able to elucidate the primary formation pathways of HOM (Rissanen et al., 2014; Jokinen et al., 2014; Mentel et al., 2015). We also note that the HOM-related terminology has evolved over the last years, and here we define HOM as organic molecules formed through gas-phase autoxidation, containing six or more oxygen atoms.

The main process in HOM formation is peroxy-radical (RO_2) autoxidation (Crounse et al., 2013), which involves an intramolecular H-abstraction by the peroxy-radical group to form a hydroperoxide and a carbon-centered radical to which molecular oxygen (O_2) can rapidly add to form a new RO_2 with a higher level of oxygenation. The efficiency of this process is mainly determined by the availability of easily "abstractable" H-atoms, and such are often formed in the ozonolysis of endocyclic alkenes (Rissanen et al., 2014 & 2015; Berndt et al., 2015). This structural component can be found in many biogenic VOC, such as monoterpenes, enhancing their roles as SOA precursors through efficient autoxidation and HOM formation (Ehn et al., 2014; Jokinen et al., 2014; Berndt et al., 2016). Peroxy-radicals are important intermediates in nearly all atmospheric oxidation processes. The RO_2 that have undergone autoxidation will terminate to closed-shell species in similar ways as less oxidized RO_2, taking place either by unimolecular processes leading to loss of OH or HO_2, or bimolecular reactions with NO, HO_2 or other RO_2. The termination pathway strongly influences the type of HOM that can be formed, with e.g. $RO_2 + RO_2$ reactions being able to form ROOR dimers and RO_2+NO often forming organic nitrates (Ehn et al., 2014; Berndt et al., 2018). All these bimolecular reactions of peroxy-radicals, as well as the initial oxidant-VOC reaction, are temperature-dependent. For example, the reaction rate of ozone with α-pinene, a broadly studied SOA-forming system, is $6.2 \cdot 10^{17}$ ($\pm 1.3 \cdot 10^{17}$) cm^3 $molec^{-1}$ s^{-1} at 3 °C, and $8.3 \cdot 10^{17}$ ($\pm 1.3 \cdot 10^{17}$) cm^3 $molec^{-1}$ s^{-1} at 22 °C (Atkinson et al., 1982). However, the intramolecular isomerization through H-shifts is likely to have a much stronger temperature dependence, due to the higher energy barrier for the H-shift (Seinfeld and Pandis, 2006; Otkjær et al., 2018). As an example (Praske et al., 2018) reported theoretical estimates of different H-shifts in hexane-derived RO_2 which increased roughly by

a factor of 5 to10 when the temperature increases by 22 °C (from 23 °C to 45 °C). Possible changes in HOM formation as a function of temperature are thus expected to derive mainly from changes in the autoxidation process. However, a detailed mechanistic understanding the various autoxidation steps, let alone their temperature dependencies, is still lacking for most atmospheric VOC-oxidant systems, owing partly to the plethora and the complexity of the possible reaction pathways.

Despite recent work in determining the impact of temperature on aerosol formation (Kristensen et al., 2017; Stolzenburg et al., 2018), literature on corresponding HOM effects are extremely limited. At room temperature (i.e. 20 ±5 °C), HOM molar yields have been estimated to be some percent for most monoterpenes in reactions with ozone or OH (Ehn et al., 2014; Jokinen et al., 2015). Only very recently, studies were presented where HOM formation experiments have been conducted at varying temperatures. Stolzenburg et al. (2018) showed that at lower temperatures, the CI-APi-TOF detects much lower HOM concentrations, though no quantitative values on the HOM yields were given. The impact of decreased HOM on new-particle growth rates was compensated by less oxidized species being able to condense at the lower temperatures. In another study, Frege et al. (2018) also concluded that HOM formation decreased at lower temperatures, but their study was based on observations of naturally charged ions using an APi-TOF, complicating the interpretation of HOM formation rates.

In this study, we directly evaluate the impact of temperature on HOM yields in a laboratory chamber during α-pinene ozonolysis experiments at 20 °C, 0 °C and -15 °C. Relative changes in HOM formation are compared between temperatures both for total HOM yields as well as on a molecule-by-molecule basis. The more detailed impact of temperature on the molecular distribution of HOM is expected to provide new insights into critical steps in the formation pathways.

2. Methods

2.1. The AURA Chamber

A detailed description of the AURA chamber can be found in Kristensen et al. (2017). Essentially, it consists of a 5 m^3 Teflon® bag contained in a temperature-controlled enclosure. Configured in batch sampling mode, the chamber was initially cleaned by flushing at 20 °C with purified ambient air (i.e. filtered air exempt of particles, water vapor and VOC, and reduced NOx concentration), and subsequently set to the desired temperature and finally filled with the necessary reagents. Over the course of the experiment, it was progressively emptied due to sampling by the measuring instrumentation. In our experiments, we first added ozone to a concentration of 100 ppb, provided by an ozone generator (Model 610, Jelight Company, Inc.) after which the oxidation reaction started when the VOC was introduced by vaporization of a calculated volume of liquid reagent (α-pinene or β-pinene) into a hot stream of nitrogen, reaching the desired VOC concentration (10 or 50 ppb).

2.2. The ACCHA Experiment

The Aarhus Chamber Campaign on HOM and Aerosols (ACCHA) experiment aimed to explore oxidation processes and aerosol formation during dark monoterpene ozonolysis at different temperatures, from -15 °C to 20 °C. The experiments focused on α-pinene oxidation at two different concentrations (10 ppb and 50 ppb) for three different temperatures: -15 °C, 0 °C and 20 °C. Two additional experiments were conducted with temperatures ramped from the coldest to the warmest or reversely during experiments at 10 ppb of α-pinene. For comparison, fixed temperature runs were also performed using β-pinene, at a concentration of 50 ppb. Ozone (100 ppb) was used as the main oxidant, but hydroxyl radicals also took part in the oxidation reactions as OH-scavengers were not employed in the experiments discussed here. According to model simulations using the master chemical mechanism v3.3.1 (Jenkin et al., 1997 & 2015; Saunders et al., 2003), ozonolysis accounted for approximately 2/3 and OH-oxidation for 1/3 of the α-pinene oxidation respectively. A table summarizing the experiments of the campaign can be found in the Appendix (Table A1).

156

157 **2.3. Instrumentation**

158 The ACCHA experiment involved a diverse set of instruments measuring both the gas phase and the particle
159 phase. The gas phase instrumentation included a Proton Transfer Reaction Time Of Fight Mass Spectrometer
160 (PTR-TOF-MS, Model 8000-783, IONICON Inc., Jordan et al., 2009) for measuring the concentrations of the
161 injected VOCs and other volatile products, as well as a nitrate-based Chemical Ionization Atmospheric
162 Pressure interface Time of Flight (CI-APi-TOF, TOFWERK A.G. & Aerodyne Research Inc., Jokinen et al.,
163 2012) mass spectrometer, analyzing the highly oxidized organic products of lower volatility (e.g. HOM). The
164 CI-APi-TOF is described in more detail in the following section. The aerosol phase measurement was done
165 using (1) a nano-Condensation Nuclei Counter (nCNC), being a combination of a Particle Size Magnifier
166 (PSM, Model A10, Airmodus Ltd.) and a Condensation Particle Counter (CPC, Model A20, Airmodus Ltd.),
167 (2) a Scanning Mobility Particle Sizer (SMPS; Kr-85 neutralizer (Model 3077A, TSI), electrostatic classifier
168 (Model 3082, TSI), nano-water-based CPC (Model 3788, TSI)), counting the size resolved particles from 10
169 nm to 400 nm, (3) a High Resolution Time-Of-Flight Aerosol Mass Spectrometer (HR-TOF-AMS, Aerodyne
170 Research Inc., Jayne et al., 2000) determining the chemical composition of non-refractory aerosol particles
171 larger than ~35 nm. The temperature and relative humidity inside the chamber were monitored using HC02-
172 04 sensors (HygroFlex HF320, Rotronic AG), and the ozone concentration was measured with an ozone
173 monitor (O_3-42 Module, Environment S.A.).

174

175 **2.4. Measuring highly oxygenated organic molecules in the gas phase**

176 HOM present in the gas phase were measured using a CI-APi-TOF mass spectrometer. The instrument sampled
177 air at about 80 cm from the wall of the chamber via a ¾ inch tube directly connected to the CI-APi-TOF, which
178 was located outside the chamber enclosure (~20 °C at all time). The sheath air (taken from a compressed air
179 line) was 30 LPM and the total flow (generated by the house vacuum line) was 40 LPM. The ~1 m long inlet
180 had a flow of 10 LPM caused by the difference between the sheath and total flows. With such a tube length
181 and flow, roughly half of the HOM are expected to be lost to the walls of the inlet lines. The CI-APi-TOF is
182 described by Jokinen et al. (2012), but also briefly presented here. Strong acids and highly oxygenated organic

183 molecules have been shown to cluster efficiently with nitrate ion (Ehn et al., 2014; Hyttinen et al., 2015).
184 Nitrate ions (i.e. NO_3^-, $HNO_3NO_3^-$ and $(HNO_3)_2NO_3^-$), produced by exposure of nitric acid vapors to soft X-
185 ray radiation, were electrostatically introduced into the sample flow of 10 LPM with a reaction time of roughly
186 200 ms at atmospheric pressure.
187 The ions, clusters with NO_3^-, were sampled through a 300 µm critical orifice into the APi, where ions were
188 guided and focused by two segmented quadrupoles through chambers with gradually decreasing pressures (~2
189 mbar and ~10^{-2} mbar, respectively). Finally, an ion lens assembly, at ~10^{-5} mbar, guided the ions into the TOF
190 chamber (~10^{-6} mbar) where they were orthogonally extracted and their mass-to-charge ratios determined. The
191 detected signal of each ion is then expressed as counts per second (cps) or counts per second normalized by
192 the sum of reagent (nitrate) ions (norm. cps). More detail about the APi-TOF itself can be found in Junninen
193 et al. (2010). Quantification of HOM remains challenging, and, in this work, we aim at explaining the relative
194 changes of HOM measured at different temperature rather than focusing on their absolute concentration.
195 However, in some instances, we also estimate absolute quantities by applying a calibration factor C = 1.65 ·
196 10^9 molecules cm^{-3}, (cf. Jokinen et al., 2012, for details on C). This translates to ~70 ppt of HOM per
197 normalized counts. As no calibrations were performed during the ACCHA experiments, the value was taken
198 from a sulfuric acid calibration (methodology according to Kürten et al., 2012) performed during an earlier
199 measurement campaign. While associated with a large uncertainty (estimated to be at least -50 % / +100 %)
200 using this value, we obtained HOM molar yields (as described in later sections) of a similar range as earlier
201 studies (Jokinen et al., 2012; Ehn et al., 2014). We estimated a detection limit from our experimental data at
202 the lowest temperature to be roughly 10^{-5} normalized counts, which correspond to ~10^4 molecules cm^{-3}.
203

204 **2.5. HOM dynamics in a batch mode chamber**

205 Being configured in batch mode, without active mixing, the AURA chamber is a dynamic reactor where
206 concentrations of products are a function of cumulative sources and cumulative sinks from the start of the
207 experiment. In the case of HOM, their lifetime in the gas phase must be short due to their low vapor pressure
208 and, thus, their fast condensation. This means that the measured HOM concentrations are mainly the result of
209 production and loss having occurred within the previous minutes, as described in more detail in the following
210 section.

The temporal change in HOM concentrations (i.e. $\frac{d[HOM]}{dt}$) can be expressed as the sum of the production terms and loss terms. The HOM formation is governed by the VOC reaction rate while the loss is dominated by condensation onto particles or walls. For the yield estimation analysis, we focus mainly on the high concentration experiments (i.e. [α-pinene] = 50 ppb), where the high condensation sink (CS, on the order of 0.1 s^{-1}) will dominate over the wall loss rate. In a smaller chamber with active mixing, the wall loss rate for low-volatile species has been estimated to be around 10^{-2} s^{-1} (Ehn et al., 2014), and in the AURA chamber we expect it to be much slower, likely on the order of 10^{-3} s^{-1}. Therefore, we can formulate simplified expression as in the following equations:

$$\frac{d[HOM]}{dt} = \gamma_{HOM} \cdot k \cdot [VOC] \cdot [O_3] - CS \cdot [HOM] \qquad (Eq. 1)$$

$$\gamma_{HOM} = \frac{\frac{d[HOM]}{dt} + CS \cdot [HOM]}{k \cdot [VOC] \cdot [O_3]} \qquad (Eq. 2)$$

Herein, γ_{HOM} corresponds to the HOM yield. The temperature-dependent rate constant of α-pinene ozonolysis, k, was taken to be $8.05 \cdot 10^{-16}$ $e^{-640/(273.15+T)}$ cm^3 $molecules^{-1}$ s^{-1}, where T is the temperature in degrees Celsius, (Atkinson, 2000; Calvert et al., 2002). Since the majority of HOM are irreversibly lost upon contact with a surface (Ehn et al., 2014), the CS represents the total sink at a time t. The CS was estimated using the measured particle number size distributions from the SMPS (Dal Maso et al., 2005). The molecular properties that govern the CS are the mass accommodation coefficient, the molecular diffusion coefficient and the mean molecular speed. Based on the work by Julin et al. (2014), the mass accommodation coefficient was set to unity. The molecular diffusion coefficient was calculated using Fuller's method (Tang et al., 2015) and the mean molecular speed was calculated using kinetic theory. Both the molecular diffusion and speed depends on molecular composition and on the absolute temperature during the experiments. $C_{10}H_{16}O_7$ was taken as a reference for the CS estimation, being one of the most abundant HOM. In comparison, the CS calculated for the largest molecules (i.e. HOM dimers) were approximately 30 % lower. With the aforementioned

assumptions, a distinct yield for each identified HOM of interest can be derived based on Eq. 2, as the slope of a linear fit to the data during an experiment, with $k \cdot [VOC] \cdot [O_3]$ on the x-axis and $\frac{d[HOM]}{dt} + CS \cdot [HOM]$ on the y-axis.

3. Results & Discussion

3.1. Effect of the temperature on the CI-APi-TOF

Since this work targets the variation of HOM in relation to temperature, it is necessary to assess the reliability of the CI-APi-TOF measurement towards temperature variations. The sensitivity towards a certain molecule depends to first approximation on the charging efficiency in the CI inlet and the transmission efficiency of the sampled ion in the APi-TOF. The charging efficiency of a HOM is primarily determined by the stability of the HOM $\cdot NO_3$- cluster relative to the HNO3 $\cdot NO_3$- cluster (Hyttinen et al., 2015), and we do not expect temperature to cause a large difference in this relative behavior. However, the transmission can be sensitive to small changes, and especially pressures inside the instrument are important to monitor, as the optimal voltages guiding the sampled ions through the instrument have been tuned for specific pressures. The pressures of the two quadrupole chambers (named "SSQ" and "BSQ", respectively, where the pressure dependence is the largest) as well the Total Ion Count (TIC, i.e. sum of all signals), the Reagent Ion Count (RIC, i.e. sum of nitrate ion signals) and the contributions of each nitrate ion signals are presented in Figure 1. The SSQ pressures (Fig. 1a) were found relatively stable (average: ~2.07 mbar) and the BSQ averaged pressure (Fig. 1b) was ~$3.3 \cdot 10^{-2}$ mbar, which are typical values for this instrument. Unfortunately, the other instrumental pressures (i.e. ion lens assembly chamber or TOF chamber pressures) were not recorded due to sensor failures. However, as these chambers are at low enough pressures that ion-gas collisions are very rare, any possible small variations in the pressures are unlikely to affect our results. When going from the coldest temperature (-15 °C) to the highest (20 °C), in a continuous temperature ramp, the SSQ pressure decreased by ~0.01 mbar, corresponding to a relative change of 0.5 % (Fig. 1a). Over the same temperature range, the pressure within the second chamber (BSQ) decreased by ~$1.5 \cdot 10^{-3}$ mbar (~4.5 %) when the temperature varied by 35 °C (Fig.

1a). The same characteristics were observed when comparing across experiments performed at constant temperatures and for the continuous temperature ramping experiments. The SSQ pressure values below 2.02 mbar at -15 °C and 20 °C, corresponding also to the lowest BSQ pressures measured, were related to particularly low ambient pressures (~981.8 mbar). Thus, the effect of temperature within the AURA chamber caused smaller variability of the internal pressures than ambient pressure changes.

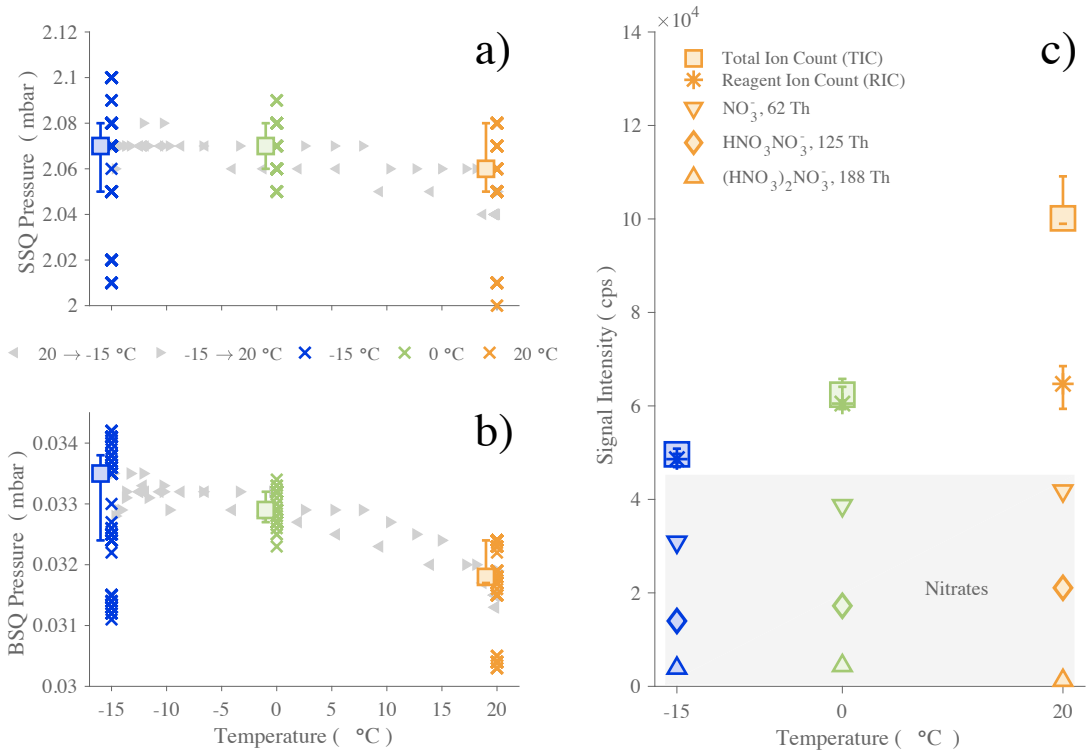

Figure 1: Evolution of the CI-APi-TOF pressures in the first (a) and second (b) quadrupole chambers (SSQ and BSQ, respectively) and signal counts (c) as a function of temperature in the AURA chamber. The APi pressures (panels a & b) are represented by crosses, depicting 10-minute averaged data points for all α-pinene ozonolysis experiments, colored by temperature (blue for -15 °C, green for 0 °C and orange for 20 °C). The squares are the median values for each temperature with their 75th and 25th percentiles. Additionally, the gray triangles relate the data (10-minute averages) of two temperature ramp experiments, from -15 °C to 20 °C (right-pointing triangles) or from 20 °C to -15 °C (left-pointing triangles). Panel c) shows averages of the sum of all ion signals (TIC, square-markers) and the sum of all reagent ion signal (RIC, asterisks-markers). RIC markers also include 25th and 75th percentiles. Nitrate signal contributions are also included separately (markers in gray-shaded area: down pointing triangle for NO_3^-, diamond marker for $HNO_3NO_3^-$ and triangle pointing upward for $(HNO_3)_2NO_3^-$).

The RIC signal (Fig. 1c) stayed within the range 5-7 · 10^4 cps, with its lowest values observed at -15 °C. The comparatively larger increase in TIC at the highest temperature is mainly explained by the fact that much higher HOM concentrations were formed at 20 °C compared to lower temperature experiments, and the transmission at these masses is generally higher than in the region of the reagent ions (Junninen et al., 2010; Ehn et al., 2011; Heinritzi et al., 2016). We conclude from the above investigations that changes on the order of tens of percent, based on the variation in RIC, occurred in our instrument as the AURA chamber temperature was varied, and that only signal changes larger than this should be attributed to actual perturbations in the chemistry taking place in the chamber.

3.2. Ozonolysis reaction in the AURA chamber: a typical α-pinene experiment at 20 °C

Selected gas phase precursors and products, including aerosols, for a high-load (i.e. 50 ppb, during 12-Jan-2017) α-pinene oxidation experiment at 20 °C are shown in Figure 2. The steep increase in α-pinene concentration, measured by PTR-TOF-MS, indicates the start (defined as time 0) of the oxidation reaction experiment (Fig. 2a). The formed aerosol product, i.e. particle number and aerosol mass, are presented in Fig. 2c. Herein, we observe an increase of the aerosol mass over the first two hours of the experiment whereas the particle number concentration plateaued in the first ten minutes after VOC injection. On the other hand, the HOM signals (Fig. 2b) show a large increase immediately as the VOC was injected. A smaller increase was also observed when the ozone was introduced, most likely due to residual volatiles reacting with ozone inside the chamber. After the first 10 min, HOM signals start to decrease as the CS (Fig. 2d) rapidly increases under these high aerosol loads. After the first half hour, the CS only changes by some tens of percent, while the VOC oxidation rate (gray crosses in Fig. 2b) decreases around one order of magnitude over the following hours of the experiment. Therefore, concentrations of low-volatile HOM should largely track the decay rate of the VOC oxidation rate, which is also observed. We observe a slower decay of HOM monomers than dimers, suggesting that some of the monomers may be semi-volatile enough to not condense irreversibly upon every collision with a surface, and/or that the VOC oxidation rate also influences the formation chemistry, as discussed in more detail in later sections.

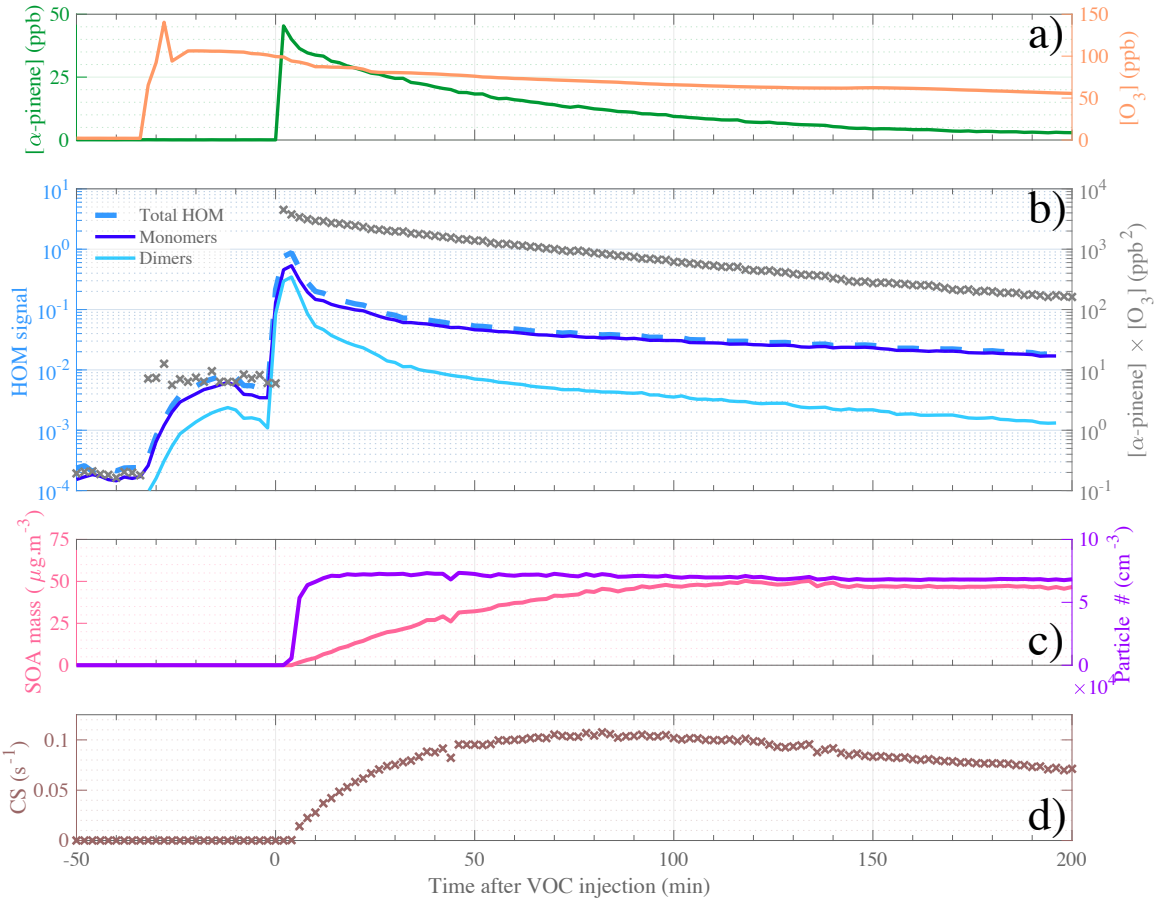

Figure 2: Temporal evolution of the main parameters during a typical α-pinene ozonolysis experiment (initial conditions: [α-pinene] = 50 ppb, [O_3] = 100 ppb, T = 20 °C). Reactant concentrations are shown in Panel a, with α-pinene concentration in dark green and ozone concentration in orange. HOM signals are plotted in Panel b, with a distinction between Total HOM (dashed medium-blue line), HOM monomers ($C_{10}H_{14-16}O_{7-11}$, dark blue line) and HOM dimers ($C_{19-20}H_{28-32}O_{10-18}$ light blue line), as well as the product [α-pinene] · [O_3] represented by gray cross markers. Panel c depicts the SOA mass (pink line) and the particle concentration (purple line). Panel d shows the evolution of the condensation sink. The time span (in x-axis) is expressed as minutes after α-pinene injection, thus the time zero represents the start of the experiment.

For a more detailed investigation at the HOM formation upon the reaction between ozone and α-pinene, we compare compounds observed in the range between 300 – 600 Thomson (Th) in the CI-APi-TOF, during a background measurement before and 10 min after α-pinene injection for each temperature (Figure 3). The

largest HOM signals, highlighted in darker colors, are primarily observed at the highest temperature, but also in the monomer area (300 – 375 Th). The dimer signals (between 450 – 600 Th) are smaller, but still contribute significantly to the total HOM concentration. With the exception of the -15 °C experiment where HOM dimers already reach the background level after 10 min, all molecules selected as representative HOM are present in all the spectra. The detailed peak list of HOM compounds, selected for their high signal intensity, including exact masses and elemental composition is provided in the Appendix (Table A2).

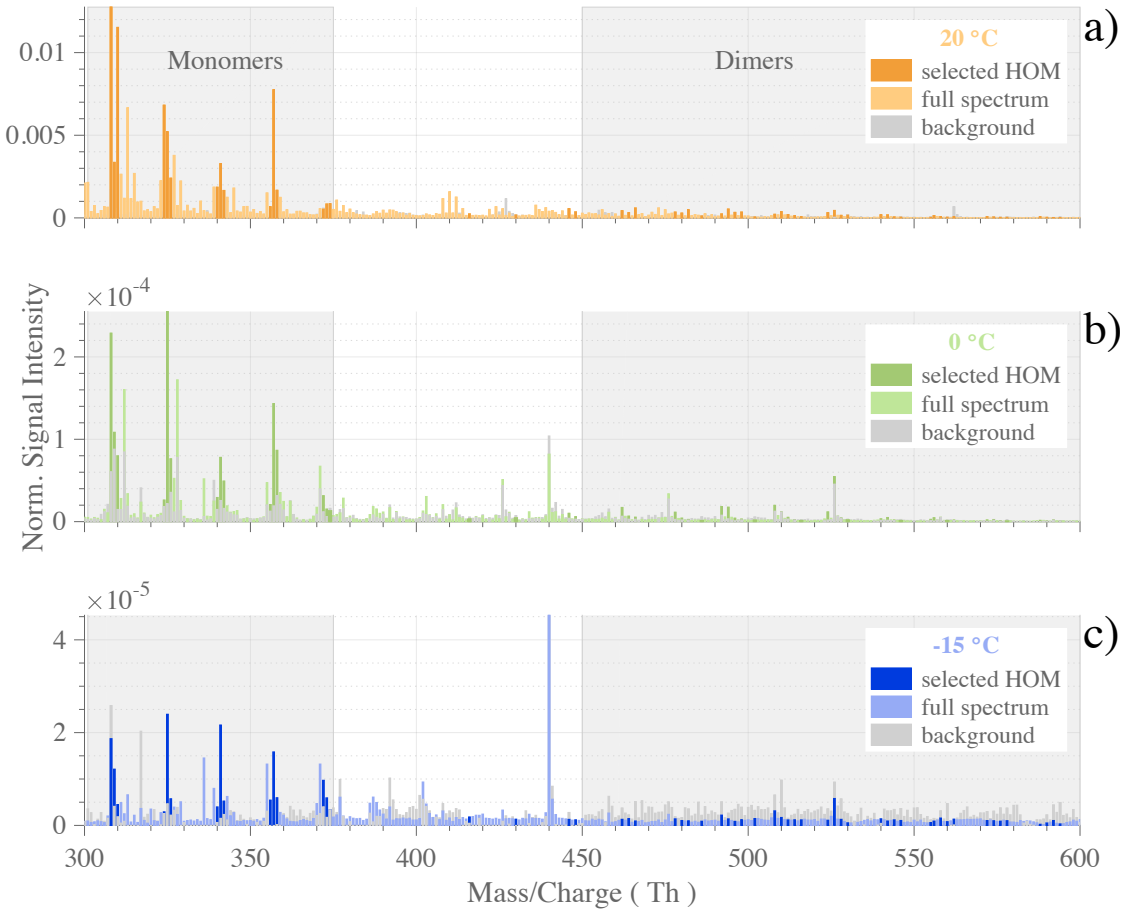

Figure 3: Typical HOM mass spectra observed during α-pinene ozonolysis experiments (initial conditions: [α-pinene] = 50 ppb, [O3] = 100 ppb,) at T = 20 °C (panel a) in orange, T = 0 °C (panel b) in green, T = -15 °C (panel c) in blue. The normalized signals were averaged over 5 minutes during background measurement before VOC injection (gray bars), and

from 40 min to 120 min after α-pinene injection (colored bars). Specific masses, selected for representing high-intensity HOM, are highlighted in darker colors. Gray-shaded areas show HOM sub-ranges of monomers and dimers.

3.3. Effect of the temperature on measured HOM

We performed a total of twelve α-pinene ozonolysis experiments with seven at high loading (i.e. [α-pinene] = 50 ppb), out of which two were conducted at 20 °C, two at 0 °C and three at -15 °C. Three experiments were performed with [α-pinene] = 10 ppb – one for each aforementioned temperature. Experiments with 50 ppb of β-pinene were also performed at the same three temperatures (see Table A2). An overview of HOM measurements for the different experiments is shown in Figure 4, with distinction between HOM monomers (Fig. 4a) and dimers (Fig4. b) as defined earlier.

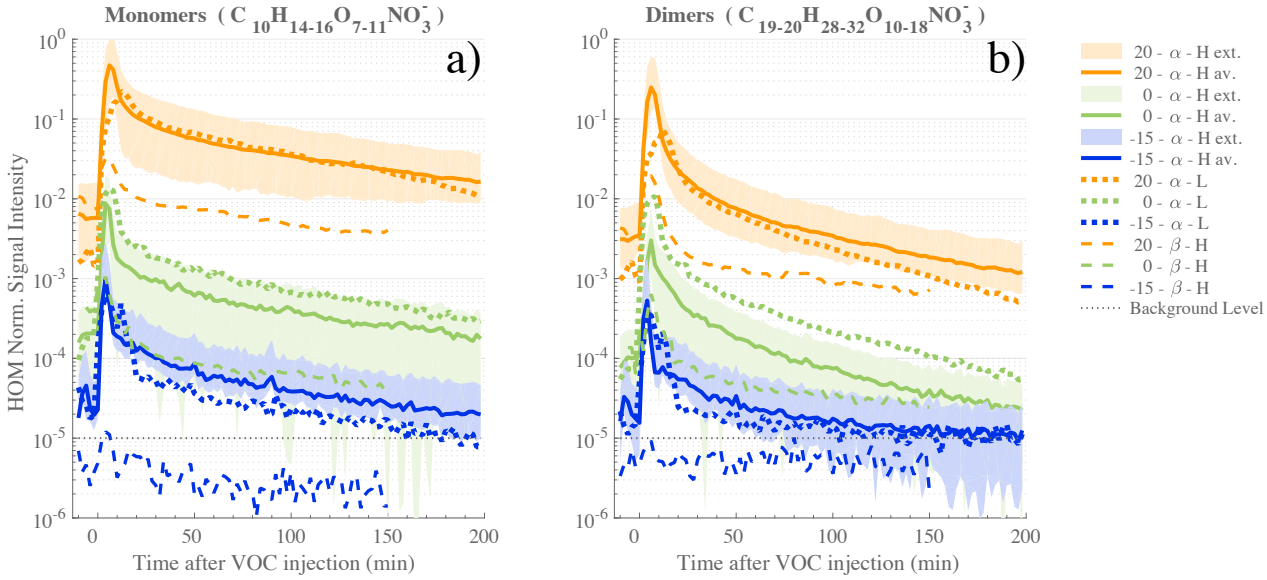

Figure 4: Time series of HOM measured during the ACCHA campaign. HOM monomer (a) and dimer (b) traces include compounds with a chemical composition of $C_{10}H_{14\text{-}16}O_{7\text{-}11}$ and $C_{19\text{-}20}H_{28\text{-}32}O_{10\text{-}18}$, respectively. The series are colored based on temperature, orange for 20 °C experiments, green for 0 °C and blue for -15 °C. Statistics over α-pinene ("α" in the legend) high load (50 ppb, "H") experiments are shown, with averaged values ("av." in continuous line) and the maximum and minimum values of the measured HOM signal (bounded shaded area). α-pinene low load (L) experiments are symbolized with colored dotted lines and the β-pinene ("β") experiments by dashed lines. The gray dotted line depicts the estimated background level of the CI-APi-TOF.

For a similar experiment type (i.e. same initial VOC concentrations), it can be seen that the resulting HOM concentrations were considerably impacted by the temperature at which the oxidation reaction occurred. The signal intensity for HOM monomers from α-pinene measured 30 minutes after the VOC injection was roughly two orders of magnitudes higher at 20 °C compared to 0 °C, and about three orders of magnitude higher compared to the -15 °C experiment. Very similar behavior is observed with respect to temperature for the dimer species as well, but with the differences that (1) less dimers are found in comparison to the HOM monomers and (2) HOM dimer concentrations are found to decrease at a faster rate during the experiment. The faster decrease of dimers compared to monomers results either from a lower production or a higher loss for dimers towards the end of the experiments. We expect that the reduced [α-pinene] and [O_3], leading to slower oxidation rates and consequently lower [RO_2] will have a greater impact on the dimers than the monomers, as the formation rate of dimers is proportional to $[RO_2]^2$, while monomers can still be formed efficiently via other RO_2 termination pathways, as discussed earlier.

When comparing the high (50 ppb) and low (10 ppb) loading α-pinene experiments, HOM signals were within the same range of concentration, and even higher at 0 °C the HOM were even more abundant in the low initial VOC concentration. Although this result may seem surprising at first, it only verifies our assumptions in Eq. 1 that the HOM concentration is a relatively simple function of formation and loss rates. Despite the fact that the low-concentration experiments had five times lower [VOC] (and consequently five times lower HOM formation rate), the condensation sink, being the primary loss for HOM, was ~8 times due to reduced aerosol formation. In other words, the loss rates decreased more than the formation rate when the precursor concentration was lowered, resulting in an increase of [HOM].

Finally, the use of β-pinene as HOM precursor produced significantly less HOM, with concentrations being more than a factor of 10 lower compared to experiments performed with α-pinene at the same conditions. This agrees with earlier studies (Jokinen et al., 2014; Ehn et al., 2014) which have shown clearly lower HOM yields for β-pinene compared to α-pinene ozonolysis. The difference is primarily attributed to the exocyclic double

bond in β-pinene. Note that, the β-pinene HOM concentrations at the lowest temperature, -15 °C, were below the instrumental limit of detection.

3.4. Yield estimation and temperature influence for molecule-specific HOM

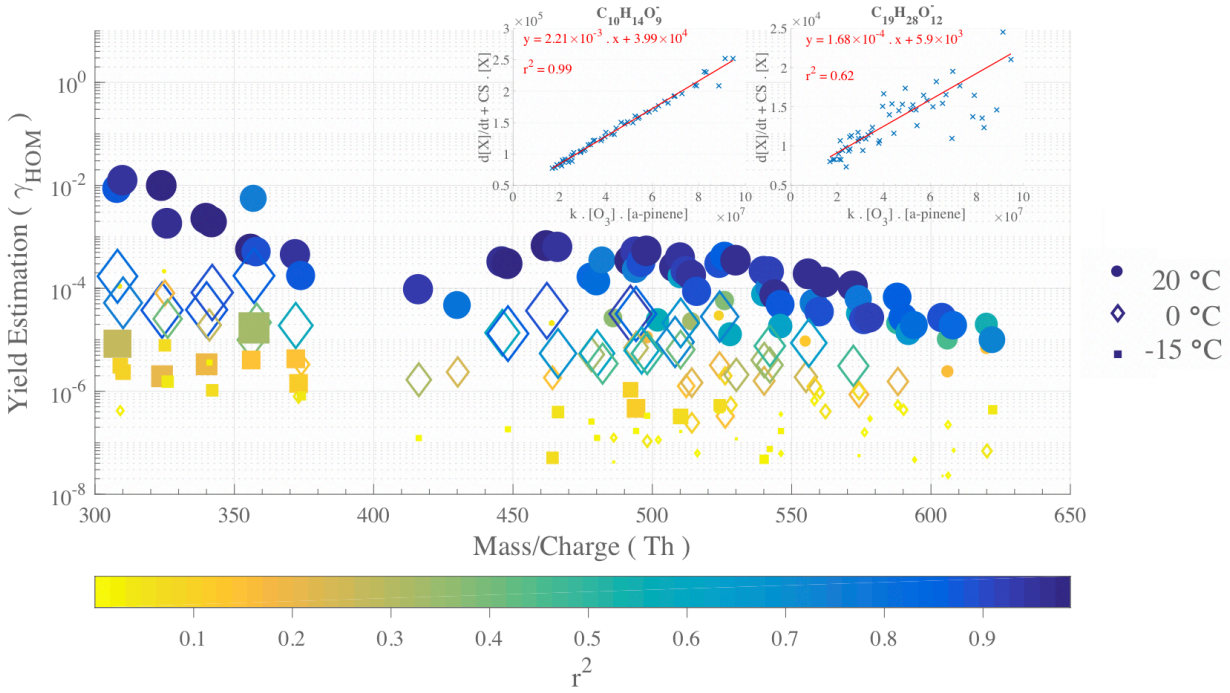

Figure 5: Yield estimations for individual α-pinene HOM from linear fits at 20 °C, 0 °C and -15 °C, from 40 to 120 min after α-pinene injection. Filled circles symbolize data from a 20 °C experiment (12-Jan-2017), diamond symbols illustrate 0 °C data (16-Jan-2017), and the filled squares represents -15 °C data (13-Jan-2017). The markers are colored and sized by r^2 values, coefficient of determination, evaluating the goodness of the linear fit used to derive the yields. The top-right insets show two examples (for $C_{10}H_{14}O_9$ and $C_{19}H_{28}O_{12}$ at 20 °C) of the yield determination by robust linear fits to the variables described in the methods section.

We determined yield estimates, individually for each HOM of interest, from the results of a robust linear fit as described in the methods section and Eq. 2. We performed the fit with 2-min averaged data points from 40 min to 120 min after the VOC injection. The yield results are shown in Figure 5, with fit examples shown for $C_{10}H_{14}O_9$ and $C_{19}H_{28}O_{12}$ in the insets. As expected, based on Figure 4, the retrieved yield values (γ_{HOM})

decrease considerably with colder reaction conditions, with a total HOM yield (i.e. sum of the individual yields for each temperature) found to be 5.2 % at 20 °C, 0.10 % at 0 °C and $6.3 \cdot 10^{-3}$ % at -15 °C.

We again emphasize the large uncertainties in these molar yield estimations, but the HOM yield values for T = 20 °C does agree well with earlier reported values (e.g. Ehn et al. (2014), Jokinen et al. (2014), Sarnela et al. (2018)). As the largest contribution to the HOM yield comes from the least oxidized monomers (e.g. high signal intensity at 308 Th and 310 Th for $C_{10}H_{14}O_7$ and $C_{10}H_{16}O_7$ respectively), the molar yield may be slightly over-estimated, especially at 20 °C, due to the loss rates possibly being lower than assumed if these HOM are not condensing irreversibly onto the aerosol. γ_{HOM} values are on average higher for HOM monomers than for dimers, with the overall shape of the distribution closely resembling the mass spectrum in Figure 3. We performed the same calculation for the experiment were [α-pinene] = 10 ppb and found total HOM-yields in the same range, as the numbers found at 50 ppb, considering our estimated uncertainty: 8.8 % at 20 °C, 0.25 % at 0 °C and $5.5 \cdot 10^{-3}$ % at -15 °C. The slightly higher values may indicate that at the higher loadings, bimolecular RO_2 termination reactions are already occurring so fast that autoxidation is hampered. The total HOM yield decrease when going from 20 °C to 0 °C decreased by a factor 50 at the higher loadings, while the corresponding value at lower loadings was 35.

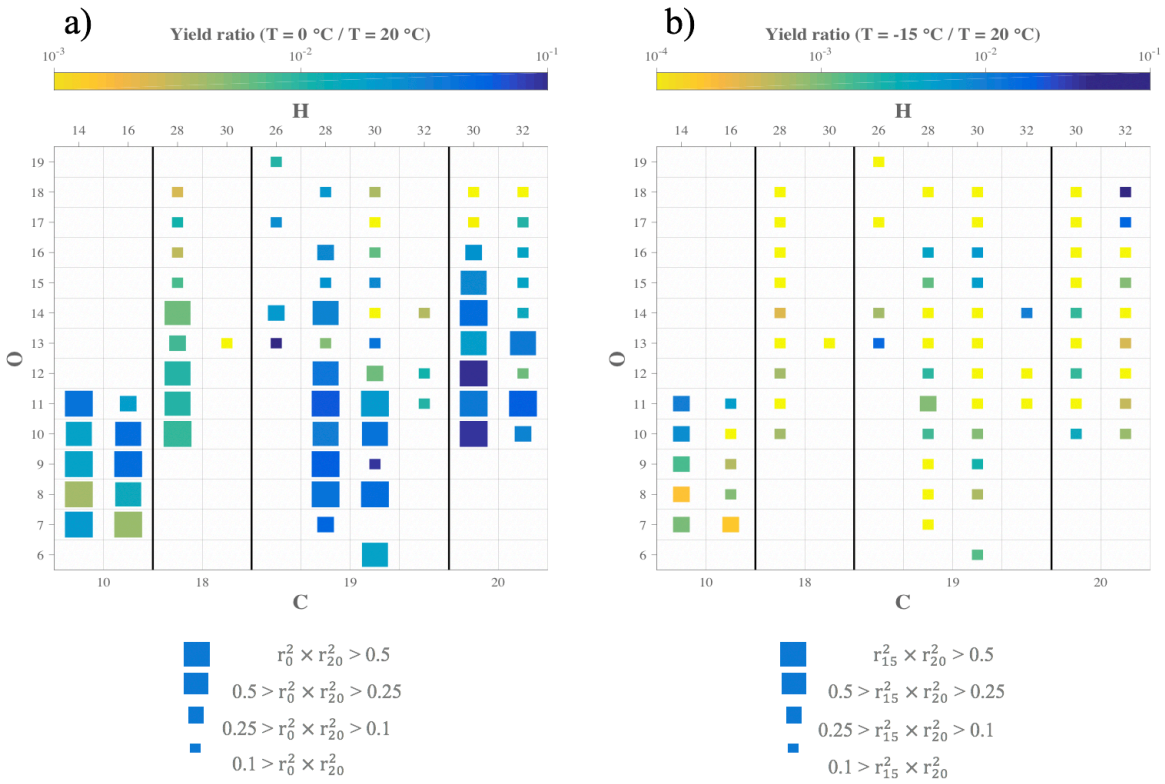

Figure 6: Comparison of yields for specific HOM compositions at different temperatures. Each square symbolizes a specific HOM measured by the CI-APi-TOF. The elemental composition can be read by taking the number of C atoms from the bottom axis, the number of H atoms from the top axis, and the number of O atoms from the left axis. The size of the square depicts the goodness of fit (r^2) used to derive the yields, and color shows the ratio of the yield at 0 °C (Panel a) or -15 °C (Panel b) compared to the yield measured at 20 °C.

While Figure 5 showed the estimated yields for every HOM at every temperature probed, specific chemical composition cannot be read from the plot. In order to assess the impact of temperature of the yield of HOM based on each elemental composition, Figure 6 depicts for each compound the ratio of the yield at 0 °C (Fig. 6a) or -15 °C (Fig. 6b) compared to the yield at 20 °C for a high load experiment of α-pinene ozonolysis. In Fig. 6a, many larger squares are observable, indicating a good reliability of our comparison analysis, but in Fig. 6b, it is clear that the HOM concentrations at the lowest temperature were too low to provide much reliable compound-specific information. From Fig. 6a we see no clear trend in the yield change for any column (i.e. changing oxygen content HOM with a given amount of C and H). The HOM yields yield ratios between the two temperatures are primarily within 10^{-2} – 10^{-1}, meaning that the molecule-specific yields dropped to between 1-10 % when temperature decreased from 20 °C to 0 °C. If autoxidation of RO_2 decreased this

considerably, one could have expected the more oxygenated HOM to decrease more than the less oxygenated ones. However, this did not seem to be the case, as e.g. some of the most abundant HOM $C_{10}H_{14}O_7$, $C_{10}H_{14}O_9$, and $C_{10}H_{14}O_{11}$ seemingly decreased the same amounts.

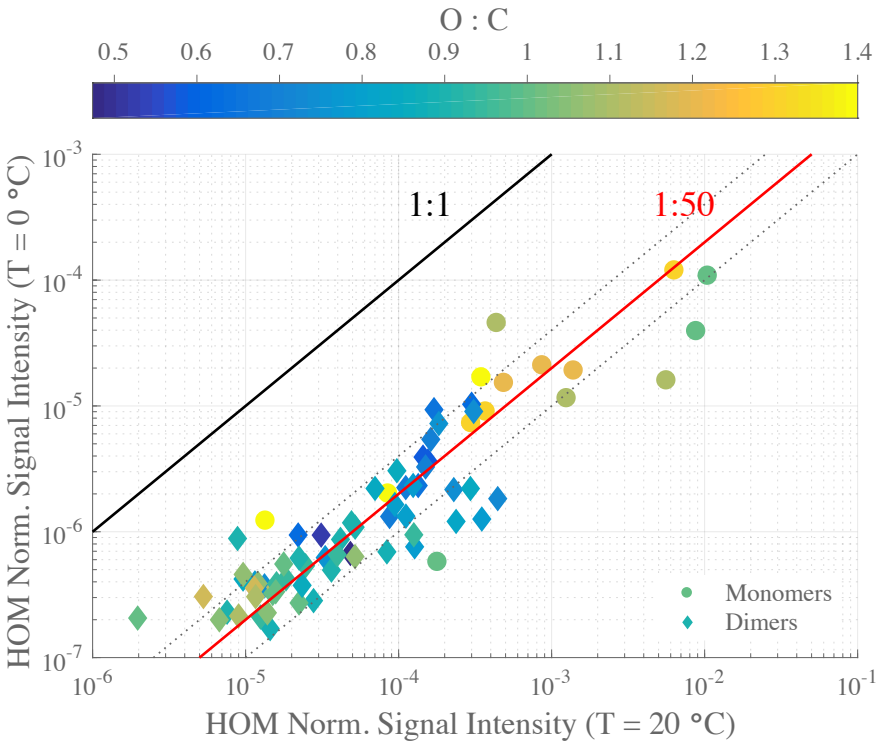

Figure 7: Scatter plot of HOM normalized signal intensity at 0°C and at 20 °C. The data points are colored by oxygen-to-carbon ratio with distinction between monomer – circle markers - and dimer compounds – diamond markers. Guide lines were added as indicators: 1:1 line – in black, 1:50 line – in red ,1:25 and 1:100 lines - in dotted grey.

In Figure 7, we show the HOM signal intensities, molecule by molecule based on the O:C ratio, from the 20 °C-experiment compared to the one at 0 °C. The vast majority of compounds fall close to the 1:50 line, which indicates similarities in the HOM spectra at both temperatures. Additionally, the points with the largest scatter (e.g. >50 % from the 1:50-line) show no trends as a function of oxygen content, which also agrees with our observations from Figure 6. One possible interpretation of this is that the rate-limiting step in the autoxidation chain takes place in RO_2 radicals with 6 or less O atoms, which are not detected with our CI-APi-TOF, while the later H-shift reactions are fast enough that other reactions still do not become competitive. These "non-HOM" RO_2 radicals may then also be key molecules for determining the final branching leading to the different

observed HOM with 7 or more O atoms. This may shed light on one of the main open challenges (Ehn et al., 2017) in understanding HOM formation, namely how RO_2 radicals with e.g. 6, 8 and 10 O atoms can form within a second, yet the relative distribution of these three does not change if the reaction time is allowed to increase (Berndt et al., 2015). Since the O_{10}-RO_2 (or its closed shell products) are not seen to accumulate over time, our results here provide support for a pathway where the O_6- and O_8-RO_2 are to some extent "terminal" products incapable of further fast H-shift reactions, while the O_{10}-RO_2 has been formed via another branch of the reaction where the autoxidation is able to proceed further. In this branch, the O_6- and O_8-RO_2 are likely only short-lived intermediates. While in no way conclusive, this highlights the need for fast measurements of HOM formation as well as improved techniques for observing less oxidized RO_2 radicals.

The only compound group where a slight decrease can be seen as a function of O-atom content is the $C_{20}H_{30}$ dimers. Interestingly, these also show some of the smallest yield ratios of all compounds. At the same time, the level of C_{18} dimers appears to drop most of all compound groups, potentially suggesting that the mechanism through which carbon atoms were lost on the way to the C_{18} dimers was sensitive to temperature, and at 0 °C the fragmentation was less prominent. It is conceivable that the different branching at 0 °C caused some of the C_{18} dimer precursors to form C_{20} dimers instead. However, this issue would need more detailed experiments in order to verify.

The decrease in HOM yield due to slower RO_2 H-shift rates at lower temperatures was found to be very dramatic under our conditions. However, the exact magnitude of this decrease in HOM yield is determined by the processes competing with the H-shifts. Under our conditions, the RO_2 lifetime is kept quite short, both due to bimolecular ($RO_2 + RO_2$ or $RO_2 + HO_2$) reactions and collisions with particles, and therefore any reduction in H-shift rates can strongly reduce the HOM yield. Inversely, under very low loadings, the RO_2 lifetime may be long enough that the temperature decreases from 20 °C to 0 °C may cause much smaller changes in the HOM yields. If the lifetime of RO_2 radicals is clearly longer than the time needed for multiple consecutive H-shifts to take place, HOM yields would decrease only marginally with temperature. In the atmosphere, RO_2

lifetime will often be governed by NO, which means that there can exist an intricate dependence of HOM yields as a function of temperature, VOC type, VOC oxidation rate, and NO_X.

4. Conclusion

We present laboratory studies of HOM formation from monoterpene ozonolysis at different temperatures (20 °C, 0 °C, and -15 °C). Our main insight is that temperature, in the studied range, considerably impacted the HOM formation, decreasing the observed HOM yield by around 50-fold upon a decrease by 20 °C. The exact temperature dependence of HOM formation in general is likely both VOC- and loading-dependent, due to the competition between autoxidation and termination reactions, and will likely be smaller at lower loadings. While autoxidation is expected to decrease with temperature, our result is still striking as it takes place over a temperature range which is atmospherically relevant for areas where monoterpene emissions are abundant, e.g. the boreal forest. One important observation was that HOM were present at all measured temperatures with roughly similar spectral distributions. This suggested that the total HOM yield as well as the final HOM distribution are mainly determined by the first H-shift steps, i.e. in the region where the CI-APi-TOF is unable to measure. This highlights the need for more comprehensive observations of autoxidation, allowing direct observations of the critical steps determining the HOM yields and, subsequently, the production rate of low-volatile organic compounds able to form secondary organic aerosol.

Authors Contribution

M. Ehn, M. Bilde, and M. Glasius supervised the ACCHA campaign. L.L.J Quéléver, K. Kristensen, M. Bilde and M. Ehn designed the experiments. K. Kristensen and L. N. Jensen initialized the chamber for experiments. L.L.J. Quéléver performed the measurement and analyzed the gas-phase HOM. K. Kristensen and L. N. Jensen measured and analyzed the aerosol phase. K. Kristensen, B. Rosati and R. Teiwes measured and analyzed the VOCs and their semi-volatile oxidation production, also supervised by R. Bossi. M. Ehn, K. Daellenbach, O.

Peräkylä and P. Roldin guided and helped the analysis of HOM yield performed by L.L.J. Quéléver. L. L. J. Quéléver prepared the manuscript with the contribution from all co-authors.

Acknowledgments

This work was funded by the European Research Council (Grant n°: 638703-COALA), the Academy of Finland Center of Excellence program (Grant n°: 307331), Aarhus University and the Aarhus University Research Foundation. We also thank H. Skov (Aarhus University, Department of Environmental Science) for the use of the PTR-TOF-MS. We express our gratitude for the free use of mass spectrometry analysis tools: TofTools freeware provided by H. Junninen. O. Peräkylä thanks the Vilho, Yrjö & Kalle Väisälä Foundation. We also thank M. P. Rissanen and T. Kurtén for their spontaneous input on this work.

References

Atkinson, R., Winer, A., and Pitts Jr, J.: Rate constants for the gas phase reactions of O3 with the natural hydrocarbons isoprene and α-and β-pinene, Atmospheric Environment (1967), 16, 1017-1020, 1982.

Atkinson, R.: Atmospheric chemistry of VOCs and NOx, Atmospheric environment, 34, 2063-2101, 2000.

Bianchi, F., Kurtén, T., Riva, M., Mohr, C., Rissanen, M. P., Roldin, P., Berndt, T., Crounse, J. D., Wennberg, P. O., and Mentel, T. F.: Highly Oxygenated Organic Molecules (HOM) from Gas-Phase Autoxidation Involving Peroxy Radicals: A Key Contributor to Atmospheric Aerosol, Chemical Reviews, 2019.

Berndt, T., Richters, S., Kaethner, R., Voigtländer, J., Stratmann, F., Sipilä, M., Kulmala, M., and Herrmann, H.: Gas-phase ozonolysis of cycloalkenes: formation of highly oxidized RO_2 radicals and their reactions with NO, NO2, SO2, and other RO_2 radicals, The Journal of Physical Chemistry A, 119, 10336-10348, 2015.

525 Berndt, T., Richters, S., Jokinen, T., Hyttinen, N., Kurtén, T., Otkjær, R. V., Kjaergaard, H. G., Stratmann, F.,
526 Herrmann, H., and Sipilä, M.: Hydroxyl radical-induced formation of highly oxidized organic compounds,
527 Nature communications, 7, 13677, 2016.
528
529 Berndt, T., Scholz, W., Mentler, B., Fischer, L., Herrmann, H., Kulmala, M., and Hansel, A.: Accretion Product
530 Formation from Self-and Cross-Reactions of RO_2 Radicals in the Atmosphere, Angewandte Chemie
531 International Edition, 57, 3820-3824, 2018.
532
533 Calvert, J. G., Atkinson, R., Becker, K. H., Kamens, R. M., Seinfeld, J. H., Wallington, T. H., and Yarwood,
534 G.: The mechanisms of atmospheric oxidation of the aromatic hydrocarbons, Oxford University Press, 2002.
535 Crounse, J. D., Nielsen, L. B., Jørgensen, S., Kjaergaard, H. G., and Wennberg, P. O.: Autoxidation of organic
536 compounds in the atmosphere, The Journal of Physical Chemistry Letters, 4, 3513-3520, 2013.
537
538 Dal Maso, M., Kulmala, M., Riipinen, I., Wagner, R., Hussein, T., Aalto, P. P., and Lehtinen, K. E.: Formation
539 and growth of fresh atmospheric aerosols: eight years of aerosol size distribution data from SMEAR II,
540 Hyytiala, Finland, Boreal Environment Research, 10, 323, 2005.
541
542 Donahue, N. M., Kroll, J., Pandis, S. N., and Robinson, A. L.: A two-dimensional volatility basis set–Part 2:
543 Diagnostics of organic-aerosol evolution, Atmospheric Chemistry and Physics, 12, 615-634, 2012.
544
545 Donahue, N. M., Ortega, I. K., Chuang, W., Riipinen, I., Riccobono, F., Schobesberger, S., Dommen, J.,
546 Baltensperger, U., Kulmala, M., and Worsnop, D. R.: How do organic vapors contribute to new-particle
547 formation?, Faraday discussions, 165, 91-104, 2013.
548
549 Dusek, U., Frank, G., Hildebrandt, L., Curtius, J., Schneider, J., Walter, S., Chand, D., Drewnick, F., Hings,
550 S., and Jung, D.: Size matters more than chemistry for cloud-nucleating ability of aerosol particles, Science,
551 312, 1375-1378, 2006.
552

553 Ehn, M., Junninen, H., Petäjä, T., Kurtén, T., Kerminen, V.-M., Schobesberger, S., Manninen, H., Ortega, I.,
554 Vehkamäki, H., and Kulmala, M.: Composition and temporal behavior of ambient ions in the boreal forest,
555 Atmospheric Chemistry and Physics, 10, 8513-8530, 2010.
556
557 Ehn, M., Junninen, H., Schobesberger, S., Manninen, H. E., Franchin, A., Sipilä, M., Petäjä, T., Kerminen, V.-
558 M., Tammet, H., and Mirme, A.: An instrumental comparison of mobility and mass measurements of
559 atmospheric small ions, Aerosol Science and Technology, 45, 522-532, 2011.
560
561 Ehn, M., Kleist, E., Junninen, H., Petäjä, T., Lönn, G., Schobesberger, S., Maso, M. D., Trimborn, A., Kulmala,
562 M., and Worsnop, D.: Gas phase formation of extremely oxidized pinene reaction products in chamber and
563 ambient air, Atmospheric chemistry and physics, 12, 5113-5127, 2012.
564
565 Ehn, M., Thornton, J. A., Kleist, E., Sipilä, M., Junninen, H., Pullinen, I., Springer, M., Rubach, F., Tillmann,
566 R., and Lee, B.: A large source of low-volatility secondary organic aerosol, Nature, 506, 476, 2014.
567
568 Ehn, M., Berndt, T., Wildt, J., and Mentel, T.: Highly Oxygenated Molecules from Atmospheric Autoxidation
569 of Hydrocarbons: A Prominent Challenge for Chemical Kinetics Studies, International Journal of Chemical
570 Kinetics, 49, 821-831, 2017.
571
572 Frege, C., Ortega, I. K., Rissanen, M. P., Praplan, A. P., Steiner, G., Heinritzi, M., Ahonen, L., Amorim, A.,
573 Bernhammer, A.-K., and Bianchi, F.: Influence of temperature on the molecular composition of ions and
574 charged clusters during pure biogenic nucleation, Atmospheric Chemistry and Physics, 18, 65-79, 2018.
575
576 Hallquist, M., Wenger, J. C., Baltensperger, U., Rudich, Y., Simpson, D., Claeys, M., Dommen, J., Donahue,
577 N., George, C., and Goldstein, A.: The formation, properties and impact of secondary organic aerosol: current
578 and emerging issues, Atmospheric chemistry and physics, 9, 5155-5236, 2009.
579

Heinritzi, M., Hansel, A., Simon, M., Steiner, G., Wagner, A. C., Kürten, A., and Curtius, J.: submitter: Characterization of the mass-dependent transmission efficiency of a CIMS, Atmos. Meas. Tech., 9, 1449-1460, 2016.

Hyttinen, N., Kupiainen-Määttä, O., Rissanen, M. P., Muuronen, M., Ehn, M., and Kurtén, T.: Modeling the charging of highly oxidized cyclohexene ozonolysis products using nitrate-based chemical ionization, The Journal of Physical Chemistry A, 119, 6339-6345, 2015.

IPCC: Climate change 2013: the physical science basis. Contribution of the Working Group 1 to the Fifth Assessment Report (AR5) of the Intergovernmental Panel on Climate Change, edited by: Stocker, T. F., Qin, D., Plattner, G., Tignor, M., Allen, S., Boschung, J., Nauels, A., Xia, Y., Bex, V., and Midgley, P. M., Cambridge University Press, Cambridge (UK), New York (USA), 2013.

Jayne, J. T., Leard, D. C., Zhang, X., Davidovits, P., Smith, K. A., Kolb, C. E., and Worsnop, D. R.: Development of an aerosol mass spectrometer for size and composition analysis of submicron particles, Aerosol Science & Technology, 33, 49-70, 2000.

Jenkin, M. E., Saunders, S. M., and Pilling, M. J.: The tropospheric degradation of volatile organic compounds: a protocol for mechanism development. Atmospheric Environment 31, 81–104, 1997.

Jenkin, M. E., Young, J. C., and Rickard, A. R.: The MCM v3.3.1 degradation scheme for isoprene. Atmos. Chem. Phys. 15, 11433–11459, 2015.

Jimenez, J. L., Canagaratna, M. R., Donahue, N. M., Prevot, A. S., Zhang, Q., Kroll, J. H., DeCarlo, P. F., Allan, J. D., Coe, H., Ng, N. L., Aiken, A. C., Docherty, K. S., Ulbrich, I. M., Grieshop, A. P., Robinson, A. L., Duplissy, J., Smith, J. D., Wilson, K. R., Lanz, V. A., Hueglin, C., Sun, Y. L., Tian, J., Laaksonen, A., Raatikainen, T., Rautiainen, J., Vaattovaara, P., Ehn, M., Kulmala, M., Tomlinson, J. M., Collins, D. R., Cubison, M. J., Dunlea, E. J., Huffman, J. A., Onasch, T. B., Alfarra, M. R., Williams, P. I., Bower, K., Kondo,

608 Y., Schneider, J., Drewnick, F., Borrmann, S., Weimer, S., Demerjian, K., Salcedo, D., Cottrell, L., Griffin,
609 R., Takami, A., Miyoshi, T., Hatakeyama, S., Shimono, A., Sun, J. Y., Zhang, Y. M., Dzepina, K., Kimmel, J.
610 R., Sueper, D., Jayne, J. T., Herndon, S. C., Trimborn, A. M., Williams, L. R., Wood, E. C., Middlebrook, A.
611 M., Kolb, C. E., Baltensperger, U., and Worsnop, D. R.: Evolution of organic aerosols in the atmosphere,
612 Science, 326, 2009.
613
614 Jokinen, T., Sipilä, M., Junninen, H., Ehn, M., Lönn, G., Hakala, J., Petäjä, T., Mauldin Iii, R., Kulmala, M.,
615 and Worsnop, D.: Atmospheric sulphuric acid and neutral cluster measurements using CI-APi-TOF,
616 Atmospheric Chemistry and Physics, 12, 4117-4125, 2012.
617
618 Jokinen, T., Sipilä, M., Richters, S., Kerminen, V. M., Paasonen, P., Stratmann, F., Worsnop, D., Kulmala,
619 M., Ehn, M., and Herrmann, H.: Rapid autoxidation forms highly oxidized RO_2 radicals in the atmosphere,
620 Angewandte Chemie International Edition, 53, 14596-14600, 2014.
621
622 Jokinen, T., Berndt, T., Makkonen, R., Kerminen, V.-M., Junninen, H., Paasonen, P., Stratmann, F., Herrmann,
623 H., Guenther, A. B., and Worsnop, D. R.: Production of extremely low volatile organic compounds from
624 biogenic emissions: Measured yields and atmospheric implications, Proceedings of the National Academy of
625 Sciences, 201423977, 2015.
626
627 Jordan, A., Haidacher, S., Hanel, G., Hartungen, E., Märk, L., Seehauser, H., Schottkowsky, R., Sulzer, P.,
628 and Märk, T.: A high resolution and high sensitivity proton-transfer-reaction time-of-flight mass spectrometer
629 (PTR-TOF-MS), International Journal of Mass Spectrometry, 286, 122-128, 2009.
630
631 Julin, J., Winkler, P. M., Donahue, N. M., Wagner P. E., and Riipinen, I.: Near-unity mass accommodation
632 coefficient of organic molecules of varying structure. Environ. Sci. Technol., 48(20), 12083-12089, 2014.
633

634 Junninen, H., Ehn, M., Petäjä, T., Luosujärvi, L., Kotiaho, T., Kostiainen, R., Rohner, U., Gonin, M., Fuhrer,
635 K., and Kulmala, M.: A high-resolution mass spectrometer to measure atmospheric ion composition,
636 Atmospheric Measurement Techniques, 3, 1039-1053, 2010.
637
638 Kristensen, K., Jensen, L., Glasius, M., and Bilde, M.: The effect of sub-zero temperature on the formation
639 and composition of secondary organic aerosol from ozonolysis of alpha-pinene, Environmental Science:
640 Processes & Impacts, 19, 1220-1234, 2017.
641
642 Kulmala, M., Kontkanen, J., Junninen, H., Lehtipalo, K., Manninen, H. E., Nieminen, T., Petäjä, T., Sipilä,
643 M., Schobesberger, S., and Rantala, P.: Direct observations of atmospheric aerosol nucleation, Science, 339,
644 943-946, 2013.
645
646 Kürten, A., Rondo, L., Ehrhart, S., and Curtius, J.: Calibration of a chemical ionization mass spectrometer for
647 the measurement of gaseous sulfuric acid, The Journal of Physical Chemistry A, 116, 6375-6386, 2012.
648
649 Mentel, T. F., Springer, M., Ehn, M., Kleist, E., Pullinen, I., Kurtén, T., Rissanen, M., Wahner, A., and Wildt,
650 J.: Formation of highly oxidized multifunctional compounds: autoxidation of peroxy radicals formed in the
651 ozonolysis of alkenes – deduced from structure–product relationships, Atmos. Chem. Phys., 15, 6745-6765,
652
653 Otkjær, R. V., Jakobsen, H. H., Tram, C. M., and Kjaergaard, H. G.: Calculated Hydrogen Shift Rate Constants
654 in Substituted Alkyl Peroxy Radicals, The Journal of Physical Chemistry A, 122, 8665-8673, 2018.
655
656 Praske, E., Otkjær, R. V., Crounse, J. D., Hethcox, J. C., Stoltz, B. M., Kjaergaard, H. G., and Wennberg, P.
657 O.: Atmospheric autoxidation is increasingly important in urban and suburban North America, Proceedings of
658 the National Academy of Sciences, 115, 64-69, 2018.
659

660 Rissanen, M. P., Kurtén, T., Sipilä, M., Thornton, J. A., Kangasluoma, J., Sarnela, N., Junninen, H., Jørgensen,
661 S., Schallhart, S., and Kajos, M. K.: The formation of highly oxidized multifunctional products in the
662 ozonolysis of cyclohexene, Journal of the American Chemical Society, 136, 15596-15606, 2014.
663
664 Rissanen, M. P., Kurtén, T., Sipilä, M., Thornton, J. A., Kausiala, O., Garmash, O., Kjaergaard, H. G., Petäjä,
665 T., Worsnop, D. R., and Ehn, M.: Effects of chemical complexity on the autoxidation mechanisms of
666 endocyclic alkene ozonolysis products: From methylcyclohexenes toward understanding α-pinene, The
667 Journal of Physical Chemistry A, 119, 4633-4650, 2015.
668
669 Sarnela, N., Jokinen, T., Duplissy, J., Yan, C., Nieminen, T., Ehn, M., Schobesberger, S., Heinritzi, M.,
670 Ehrhart, S., and Lehtipalo, K.: Measurement–model comparison of stabilized Criegee intermediate and highly
671 oxygenated molecule production in the CLOUD chamber, Atmospheric Chemistry and Physics, 18, 2363-
672 2380, 2018.
673
674 Saunders, S. M., Jenkin, M. E., Derwent, R. G., and Pilling, M. J.: Protocol for the development of the master
675 chemical mechanism, MCM v3 (part a): tropospheric degradation of non-aromatic volatile organic
676 compounds. Atmos. Chem. Phys., 3**,** 161–180, 2003.
677
678 Stolzenburg, D., Fischer, L., Vogel, A. L., Heinritzi, M., Schervish, M., Simon, M., Wagner, A. C., Dada, L.,
679 Ahonen, L. R., and Amorim, A.: Rapid growth of organic aerosol nanoparticles over a wide tropospheric
680 temperature range, Proceedings of the National Academy of Sciences, 115, 9122-9127, 2018.
681
682 Tang, M. J., Shiraiwa, M., Pöschl, U., Cox, R. A., and Kalberer, M.: Compilation and evaluation of gas phase
683 diffusion coefficients of reactive trace gases in the atmosphere: Volume 2. Diffusivities of organic compounds,
684 pressure-normalised mean free paths, and average Knudsen numbers for gas uptake calculations. Atmos.
685 Chem. Phys., 15, 5585–5598, 2015.
686

687 Tröstl, J., Chuang, W. K., Gordon, H., Heinritzi, M., Yan, C., Molteni, U., Ahlm, L., Frege, C., Bianchi, F.,
688 and Wagner, R.: The role of low-volatility organic compounds in initial particle growth in the atmosphere,
689 Nature, 533, 527, 2016.
690
691 Zhang, Q., Jimenez, J. L., Canagaratna, M., Allan, J., Coe, H., Ulbrich, I., Alfarra, M., Takami, A.,
692 Middlebrook, A., and Sun, Y.: Ubiquity and dominance of oxygenated species in organic aerosols in
693 anthropogenically-influenced Northern Hemisphere midlatitudes, Geophysical Research Letters, 34, 2007.
694
695 Zhao, J., Ortega, J., Chen, M., McMurry, P., and Smith, J.: Dependence of particle nucleation and growth on
696 high molecular weight gas phase products during ozonolysis of α-pinene, Atmospheric Chemistry and Physics,
697 13, 9319-9354, 2013.

Appendix

Table A1 : ACCHA Experiment overview

VOC Concentration (ppb)	[VOC] reacted with O3 * (ppb)	[VOC] reacted with OH * (ppb)	Temperature (℃)	Date
		VOC : α- pinene		
50			20	12-Dec-16
50			-15	13-Dec-16
50			0	19-Dec-16
50			-15	21-Dec-16
50	30.1	15.5	20	12-Jan-17
50			-15	13-Jan-17
50	30.0	16.1	0	16-Jan-17
10	6.48	3.04	20	02-Dec-16
10			-15	07-Dec-16
10	6.30	3.14	0	08-Dec-16
10			20 → -15	09-Dec-16
10			-15 → 20	20-Dec-16
		VOC : β-pinene		
50			20	03-Jan-17
50			-15	04-Jan-17
50			0	05-Jan-17

* Estimation based on model simulations using the Master Chemical Mechanism v3.3.2 (Jenkin et al.,1997 & 2015; Saunders et al., 2003)

Table A2: Main monoterpene ozonolysis HOM products: Peak list

Monomers		**Dimers**					
m/z (Th)	Composition*	**m/z** (Th)	Composition*	**m/z** (Th)	Composition*	**m/z** (Th)	Composition*
308.06	$C_{10}H_{14}O_7$	**446.17**	$C_{19}H_{28}O_8$	**514.14**	$C_{18}H_{28}O_{13}$	**562.13**	$C_{18}H_{28}O_{16}$
309.07	$C_{10}H_{15}O_7$	**448.18**	$C_{19}H_{30}O_8$	**514.18**	$C_{19}H_{32}O_{12}$	**572.15**	$C_{20}H_{30}O_{15}$
310.08	$C_{10}H_{16}O_7$	**462.16**	$C_{19}H_{28}O_9$	**516.16**	$C_{18}H_{30}O_{13}$	**574.13**	$C_{19}H_{28}O_{16}$
324.06	$C_{10}H_{14}O_8$	**464.18**	$C_{19}H_{30}O_9$	**524.13**	$C_{18}H_{26}O_{13}$	**574.16**	$C_{20}H_{32}O_{15}$
325.07	$C_{10}H_{15}O_8$	**466.16**	$C_{18}H_{28}O_{10}$	**524.16**	$C_{20}H_{30}O_{12}$	**576.14**	$C_{19}H_{30}O_{16}$
326.07	$C_{10}H_{16}O_8$	**478.16**	$C_{19}H_{28}O_{10}$	**526.14**	$C_{19}H_{28}O_{13}$	**578.12**	$C_{18}H_{28}O_{17}$
340.05	$C_{10}H_{14}O_9$	**480.17**	$C_{19}H_{30}O_{10}$	**526.18**	$C_{20}H_{32}O_{12}$	**588.11**	$C_{19}H_{26}O_{17}$
341.06	$C_{10}H_{15}O_9$	**482.15**	$C_{18}H_{28}O_{11}$	**528.16**	$C_{19}H_{30}O_{13}$	**588.14**	$C_{20}H_{30}O_{16}$
342.07	$C_{10}H_{16}O_9$	**486.15**	$C_{17}H_{28}O_{12}$	**530.14**	$C_{18}H_{28}O_{14}$	**590.16**	$C_{20}H_{32}O_{16}$
356.05	$C_{10}H_{14}O_{10}$	**492.17**	$C_{20}H_{30}O_{10}$	**540.12**	$C_{19}H_{26}O_{14}$	**592.14**	$C_{19}H_{30}O_{17}$
357.05	$C_{10}H_{15}O_{10}$	**494.15**	$C_{19}H_{28}O_{11}$	**540.16**	$C_{20}H_{30}O_{13}$	**594.12**	$C_{18}H_{28}O_{18}$
358.06	$C_{10}H_{16}O_{10}$	**494.19**	$C_{20}H_{32}O_{10}$	**542.14**	$C_{19}H_{28}O_{14}$	**604.14**	$C_{20}H_{30}O_{17}$
372.04	$C_{10}H_{14}O_{11}$	**496.17**	$C_{19}H_{30}O_{11}$	**542.17**	$C_{20}H_{32}O_{13}$	**606.12**	$C_{19}H_{28}O_{18}$
373.05	$C_{10}H_{15}O_{11}$	**498.15**	$C_{18}H_{28}O_{12}$	**544.15**	$C_{19}H_{30}O_{14}$	**606.15**	$C_{20}H_{32}O_{17}$
374.06	$C_{10}H_{16}O_{11}$	**498.18**	$C_{19}H_{32}O_{11}$	**546.13**	$C_{18}H_{28}O_{15}$	**608.13**	$C_{19}H_{30}O_{18}$
		502.14	$C_{17}H_{28}O_{13}$	**546.17**	$C_{19}H_{32}O_{14}$	**620.10**	$C_{19}H_{26}O_{19}$
		508.17	$C_{20}H_{30}O_{11}$	**556.15**	$C_{20}H_{30}O_{14}$	**620.13**	$C_{20}H_{30}O_{18}$
		510.15	$C_{19}H_{28}O_{12}$	**558.13**	$C_{19}H_{28}O_{15}$	**622.15**	$C_{20}H_{32}O_{18}$
		510.18	$C_{20}H_{32}O_{11}$	**558.17**	$C_{20}H_{32}O_{14}$		
		512.16	$C_{19}H_{30}O_{12}$	**560.15**	$C_{19}H_{30}O_{15}$		

* Note that all compounds are detected as cluster with Nitrate Ion (NO_3^-)